Approximate impedance models for point-to-point sound propagation over acoustically-hard ground containing rectangular grooves

Approximate impedance models for point-to-point sound propagation over acoustically-hard ground containing rectangular grooves

Steve Mellish, Shahram Taherzadeh, and Keith Attenborough

Citation: The Journal of the Acoustical Society of America **147**, 74 (2020); doi: 10.1121/10.0000490
View online: https://doi.org/10.1121/10.0000490
View Table of Contents: https://asa.scitation.org/toc/jas/147/1
Published by the Acoustical Society of America

JASA ARTICLE

Approximate impedance models for point-to-point sound propagation over acoustically-hard ground containing rectangular grooves

Steve Mellish,[a] Shahram Taherzadeh, and Keith Attenborough
Faculty of STEM, The Open University, Milton Keynes, MK7 6AA, United Kingdom

ABSTRACT:
A modal model for diffraction by a contiguous array of rectangular grooves in an acoustically-hard plane is extended to predict the free space acoustic field from a point source above such a structure. Subsequently, an approximate effective impedance model for grooved surfaces is presented. Measurements have shown that these ground surfaces can be used for outdoor noise reduction but accurate modelling has required the use of computationally expensive numerical methods. The extended modal model and approximate impedance model inspired by it yield equivalent results in a fraction of the time taken by the boundary element method, for example, and could be used when designing grooved surfaces to reduce noise from road traffic. © *2020 Acoustical Society of America*. https://doi.org/10.1121/10.0000490

(Received 4 August 2019; revised 22 November 2019; accepted 27 November 2019; published online 16 January 2020)
[Editor: Yun Jing] Pages: 74–84

I. INTRODUCTION

Roughness can be used to alter the effective impedance of the surface of an acoustically hard material thereby altering the ground effect during outdoor sound propagation. It has been shown that periodic roughness consisting of identical parallel low walls or a rectangular lattice of low walls can offer a useful alternative to conventional noise barriers for surface transport noise reduction where the erection of a conventional barrier might not be acceptable.[1–3] An important effect of such roughness near grazing incidence is the creation of a surface wave.[1–4] The surface structure may be manipulated such that the resulting energy reaching the receiver can be reduced at certain frequencies and for a given source-receiver geometry by the transfer of incident sound energy into surface waves and diffraction modes.[5]

Under certain circumstances it has been found that grating structures can be represented as having an effective impedance similar to that of a porous hard-backed layer.[3] In an air-filled medium having slit-like pores with widths smaller than the incident wavelength, viscous friction and thermal exchange at the internal surfaces contribute to the surface impedance. If the gaps between the walls are larger than their height and comparable with the incident wavelength, then the main phenomenon determining sound propagation over the walls is multiple scattering. Arbitrary grating shapes may be modelled numerically using boundary element method (BEM)[6] in the frequency domain or finite difference time domain and pseudo-spectral time domain in the time domain, all of which are computationally demanding.[1,2,4]

Propagation of surface waves over rectangular grooves at ultrasonic frequencies has been investigated[3,7] using a modal approach adapted by Kelders *et al.*[7] from electromagnetic (EM) wave propagation theory formulated several decades prior by Hessel *et al.*[8] Since then, significant attention has been paid to the subject, focused primarily upon the study and manipulation of the surface waves supported by rectangularly grooved structures. Rayleigh-Bloch surface waves have been considered using modal decomposition,[9] which leads to studies of designer surface acoustic waves[10–27] that are manipulated by the design of the grooved structure in order to induce the desired response, such as acoustic collimating or focusing. Metasurfaces have been considered as profiled diffusers[15] and as phase gradient rectangularly grooved arrays to design the diffraction properties of a surface[16] leading to subsequent studies.[17–23] Similar studies relate to resonant effects in periodic arrays[24,25] and surface waves over arrays of cylinders using multiple scattering theory.[26] So far, little attention has been paid to the use of the modal model in determining an effective impedance[22] to predict point-to-point sound propagation over a grooved surface and this is the subject of the present paper.

In Sec. II, modal theory[8] is used to calculate the total field during point-to-point sound propagation over grooves and identify scattered modes that do not reach the receiver. Section III introduces a new effective impedance model in the form of a summation incorporating scattering effects. Simplified expressions for small groove widths have been suggested, but these have been found not to give as good agreement with data for the excess attenuation spectrum observed from a point source over the parallel wall or lattice surfaces as predictions using the slit-pore impedance model in the classical theory for a point source over an impedance plane.[1] Predictions of the modal model and simple summation models are compared with measurements, two-dimensional (2D) BEM numerical calculations and with predictions using

[a]Electronic mail: steve@melectronics.co.uk

https://doi.org/10.1121/10.0000490

the simplified model presented by Allard-Kelders-Lauriks[9] and slit-pore models.[28–30] Section IV offers a comparison of the various methods for some configurations that might be of interest for outdoor sound attenuation.

II. A MODAL MODEL FOR THE SOUND FIELD ABOVE RECTANGULAR GROOVED DIFFRACTION GRATINGS

A. The modal model

The modal model[6] considers the electromagnetic field scattered by a perfectly reflecting rectangular grooved surface from a homogeneous plane wave incident upon the surface with angle θ and propagation constant k. The grooved structure is assumed to be invariant in y and exhibit infinite periodicity in $\pm x$. The principle is to model the free-space field as an infinite set of discrete orthonormal modes in two dimensions with invariance in y and wave function in the x-z plane as shown in Fig. 1.

The modal model is generally applicable to similar lossless medium field problems and was applied originally to acoustics by Kelders *et al.*[7] in 1998 to investigate surface wave phenomena, although a simplified surface impedance model was published soon after.[9] The aim of this work is to use the modal model to enable predictions of point-to-point propagation over a surface containing rectangular grooves. Initially, a brief outline of the modal model is presented.

For acoustics, the field is solved in terms of the surface normal particle velocity v_z. and V_m represents the v_z amplitude for diffraction mode m. The goal of the model being to solve for the unknown V_m set. The free-space scattered field is expanded as the superposition of an infinite set of weighted Bloch-Floquet plane-wave modes ψ_m approximated by,

$$\begin{aligned}\Psi(x,z) &= V_i\,\psi_i + V_r\,\psi_r + \sum_{m\neq 0} V_m\,\psi_m,\\ \Psi(x,z) &= V_i\,e^{ik(x\sin\theta - z\cos\theta)} + V_r\,e^{ik(x\sin\theta + z\cos\theta)}\\ &\quad + \sum_{m\neq 0} V_m\,e^{j(\alpha_m x + \beta_m z)}, \quad z \geq 0,\end{aligned} \tag{1}$$

where the subscript i refers to a parameter of the incident wave, and r is the $m=0$ specularly reflected component

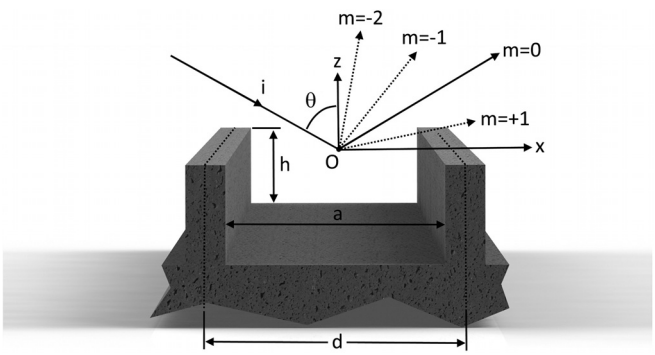

FIG. 1. Rectangular groove grating structure and diffracted modes.

with α and β being the modal wave number components in x and z. The Floquet periodic nature the problem is such that the field at $z=0$ exhibits a periodicity in d, combined with a phase constant term of the incident wave, evident in the definition of α and β,

$$\begin{aligned}\alpha_m &= k\sin\theta + \frac{2m\pi}{d},\\ \beta_m &= \sqrt{k^2 - \alpha_m^2}.\end{aligned} \tag{2}$$

Furthermore, this allows us to reduce the problem to that of solving for just one cell of the structure with extent $d/2 \geq x \geq -d/2$ so as to be evenly symmetric about the origin at $(x,z)=(0,0)$. The response of all other cells will be identical save for the $kd\sin\theta$ phase constant term of the incident wave. A real valued α_m represents a free-space propagating diffraction mode whereas an imaginary value signifies evanescence in z.

To define the problem, we require the boundary conditions at $z=0$, also posed in terms of v_z. Assuming the grooves act as closed bottom wave guides, then the resultant v_z across the aperture of the groove at $z=0$ may be considered as an infinite set of V_n weighted standing-wave mode functions of the form

$$\begin{aligned}\xi_n(x,0) &= V_n K_n \cos\left[\left(\frac{n\pi}{a}\right)\left(x+\frac{a}{2}\right)\right],\\ &\quad a/2 \geq x \geq -a/2, \quad n = 0,1,2,3,\ldots\end{aligned} \tag{3}$$

with K_n being a normalising constant. Elsewhere at the peaks of the structure, the ground is assumed acoustically hard and v_z must vanish. Truncating the number of waveguide modes to N yields an N^*N matrix of the form below, which can be solved numerically to yield a complete set of waveguide mode amplitudes V_n

$$\begin{pmatrix} A_{0,0}+A_{0,1}+\cdots+A_{0,n'} \\ A_{1,0}+A_{1,1}+\cdots+A_{1,n'} \\ \vdots \quad \vdots \quad \ddots \quad \vdots \\ A_{n,0}+A_{n,1}+\cdots+A_{n,n'} \end{pmatrix} \begin{pmatrix} V_0 \\ V_1 \\ \vdots \\ V_n \end{pmatrix} = \begin{pmatrix} X_0 \\ X_1 \\ \vdots \\ X_n \end{pmatrix}, \tag{4}$$

where A are the modal characteristic equations of the problem and X is the incident source expressions, both of which are known from the formulation of the model. Solving Eq. (4) for the V_n set defines the boundary conditions at $z=0$. Finally, truncating m to M and correlating the boundary condition at $z=0$ with each free space mode m across one period of the structure yields the set of V_m amplitudes completing the modal model solution. The resulting free space plane wave field can be plotted directly in terms of v_z from the superposition of the set of V_m weighted modes. Total pressure may then be obtained from the impedance relationship Z_m for each mode. The coupling of the free-space and waveguide modes accounts for inter-groove interaction which becomes ever more significant as the spacing between adjacent grooves reduces.

A time dependence of $e^{-i\omega t}$ is assumed and omitted throughout for clarity and, unless otherwise stated, the truncation parameters are $M = 25$ and $N = 5$.

B. Application to point-to-point propagation

For predicting point-to-point propagation, it is convenient if the grooved surface can be modelled as an effective impedance plane with normalised impedance Z_{eff} as shown in Fig. 2, where Z_{eff} is normalised to the characteristic impedance of the free-space medium Z_c.

This holds only for the geometry for which the modal model is applied because Z_{eff} depends upon the angle of incidence and source-receiver geometry. The plane wave field is accumulated from the set of M modes at the receiver location given the source receiver geometry. The origin is assumed to be the notional point of specular reflection from the surface for ease of modal summation. A geometric algorithm is introduced to limit the horizontal extent of the grooved surface to between the points x_1 and x_2 shown in Fig. 3. Free-space propagating scattered components with propagation angles such that they would not intersect the receiver are omitted from the field summation. Evanescent modes are also omitted from the plane wave summation as they are high order modes resulting from the solution of the boundary conditions imposed by the surface in the presence of homogeneous plane wave excitation. According to Tolstoy,[32] these evanescent modes differ fundamentally from true surface waves that propagate along and are supported by the structure of the surface alone and in the absence of an incident field. The propagating surface wave supported by the surface roughness and excited by a non-planar source will be accounted for by the surface wave specific term $F(w)$ in the spherical reflection coefficient Eq. (11) once applied to point-to-point propagation via Z_{eff} so long as $\mathrm{Im}(Z_{eff}) \gg \mathrm{Re}(Z_{eff})$.

Using the Kronecker delta, these conditions can be stated as

$$\delta^{\theta_1}_{\theta_2}(\theta_m) = \begin{cases} 1 & if\ \ \theta_2 \geq \theta_m \geq \theta_1 \\ 0 & if\ \ \mathrm{Im}(\theta_m) > 0 \\ 0 & else. \end{cases} \tag{5}$$

Although x_1 and x_2 may be defined freely within the limits $-\infty < x_{1,2} < \infty$ and $x_1 < x_2$ to suit the problem at hand, subsequent results will be presented for the particular case

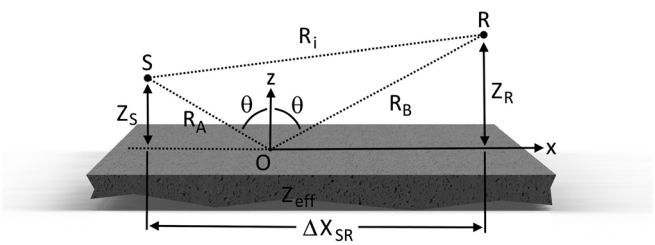

FIG. 2. Point-to-point acoustic propagation above an effective impedance plane.

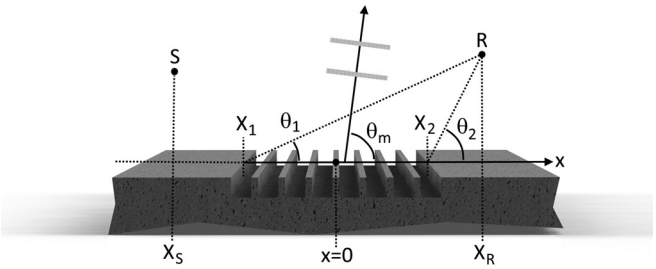

FIG. 3. Geometric modal cut-off scheme.

where the grating extends in the horizontal space between source and receiver of $x_1 = x_S$ and $x_2 = x_R$. The zero phase point of the incident wave is assumed to be coincident with the origin. Applying this method, the total acoustic pressure field at the receiver point (x_R, z_R) is approximated by the addition of the incident p_i the specularly reflected p_r and scattered p_s pressure field components thus

$$\begin{aligned} p(x_R, z_R) &= p_i(x_R, z_R) + p_r(x_R, z_R) + p_s(x_R, z_R) \\ &= Z_0 V_i \exp\left(ik(x_R \sin\theta - z_R \cos\theta)\right) \\ &\quad + Z_0 V_r \exp\left(ik(x_R \sin\theta + z_R \cos\theta)\right) \\ &\quad + \sum_{m\neq 0} \delta^{\theta_1}_{\theta_2}(\theta_m) Z_m V_m \exp\left(i(\alpha_m x_R + \beta_m z_R)\right), \end{aligned} \tag{6}$$

where the impedance relationship relating pressure to v_z for each mode is

$$Z_m = \frac{Z_c k}{\sqrt{k^2 - \left(k \sin\theta + \frac{2m\pi}{d}\right)^2}}. \tag{7}$$

From the calculated field, use is made of the plane wave reflection coefficient[33] Γ_P,

$$\Gamma_P = \frac{\cos\theta - 1/Z_{eff}}{\cos\theta + 1/Z_{eff}}. \tag{8}$$

A value for Γ_P may be deduced from the calculated pressure field as the ratio of $p_r + p_s$ and p_i as follows, including a phase constant to remove the plane wave path length difference, l_{PD}, of the incident and reflected components

$$\Gamma_P = \frac{p_r(x_R, z_R) + p_s(x_R, z_R)}{p_i(x_R, z_R) \exp\left(-ik\, l_{PD}\right)}. \tag{9}$$

Rearranging Eq. (8) for Z_{eff} as the subject and using Eq. (9) for Γ_P yields an equivalent effective impedance for the grooved surface of

$$Z_{eff} = \frac{(1 + \Gamma_P)\sec\theta}{1 - \Gamma_P}. \tag{10}$$

The effective impedance is, however, dependent upon the source-receiver geometry. The independence of wave type

https://doi.org/10.1121/10.0000490

allows us to apply Z_{eff} in the point-to-point propagation model within the spherical reflection coefficient[33] Γ_S, given as

$$\Gamma_S = \Gamma_P + (1 - \Gamma_P)F(w) \tag{11}$$

where

$$F(w) = 1 + i\sqrt{\pi}.w\,\mathrm{cef}(w)$$

w, known as the numerical distance, is

$$w = 1 + \left(i\sqrt{\frac{i}{2}kR_A + R_B}\right)\cos\theta + \frac{1}{Z_{eff}}$$

and cef() is the complex error function.

With reference to Fig. 2, the excess-attenuation EA_{dB} of the ground surface for a spherical source in decibel is

$$EA_{dB}(x_R, z_R) = 20\log\left|1 + \frac{(\Gamma_S \exp(ik(R_A + R_B)))/(4\pi(R_A + R_B))}{\exp(ikR_i)/(4\pi R_i)}\right|. \tag{12}$$

This is a method of approximating the response of a rectangularly grooved surface during point-to-point propagation except in the limit of $\theta \to \pi/2$ ($z_S \to 0$) where the definition of a finite v_z is nonsensical and would result in the prediction of infinite pressure fields. The surface acts an effective impedance and therefore can contribute to noise reduction due to ground effect with equivalent dependence upon source-receiver geometry.

III. AN EFFECTIVE IMPEDANCE MODEL

Consider the time dependent causal interactions of the ingoing and outgoing waves within a groove of the structure defined in Fig. 1. Each magnitude weighted mode may be considered separately and linearly combined to approximate an average lumped impedance at the aperture. To simplify the analysis, the groove walls are assumed initially to be thin so $a = d$. This assumption will later be relaxed by adding a specific term to account for effective porosity.

The effective impedance of a surface in the plane $z = 0$ is by definition[34]

$$Z = \frac{p}{v \cdot d\mathbf{n}}, \quad z = 0, \tag{13}$$

and will define the impedance within the groove aperture at $z = 0$ where p is pressure, v is particle velocity (positive in the positive direction of the associated axis), and $d\mathbf{n}$ is the surface normal unit vector pointing into the surface.[33] The vector $d\mathbf{n}$ is orientated in the -z direction as the surface is perpendicular to the z-axis and parallel to x. Therefore

$$v \cdot d\mathbf{n} = \text{vertical velocity into surface} = -v_z. \tag{14}$$

Reference will be made to the modal model set of z-direction wave numbers $\pm k_{zn}$, for the nth mode within the groove. In line with our convention, k_{zn}^+ represents the upward propagating components towards $z = \infty$ and k_{zn}^- the downward propagating components, towards $z = -\infty$. Therefore, $k_{zn}^+ = |k_{zn}|$ and $k_{zn}^- = -|k_{zn}|$.

The lossless and inviscid assumptions are invoked, and as such, the impedance for each groove mode n at $z = 0$ can be approximated thus by considering the down and up-going components separately

$$Z_g(n) = \frac{p_n^- + p_n^+}{(v_{zn}^- + v_{zn}^+) \cdot d\mathbf{n}}, \quad z = 0. \tag{15}$$

The p and v terms will be expanded at the origin $x = z = 0$. For this derivation, the amplitude of the nth-modal component present in the incident wave as projected across the groove aperture is required and will be termed C_n. Such a component in the incident wave will excite the associated down-going mode within the groove with z-axis wave number k_{zn}^-. Here, a simplifying assumption is made that the mode will be excited with the full v_z amplitude of the component present in the incident wave. In reality, this could only occur when the mode has the same impedance as the incident wave and $a = d$ to disregard non-orthonormal coupling between free space and groove modes. The C_n term is different from the modal model amplitude V_n, which is the resultant amplitude of mode-n formed at the aperture from the interference of the down-going and up-going reflected components within the groove. In this model, the down and up-going components are considered separately. Let C_n be approximated by the inner product of the n-modal characteristic and the incident wave normalised to a in order to retain correct amplitude scaling as

$$\begin{aligned} C_0 &= \int_{-a/2}^{a/2} \frac{1}{\sqrt{a}}\cos\left(\left[\frac{n\pi}{a}\right]\left[x + \frac{a}{2}\right]\right) \\ &\quad \cdot \frac{1}{\sqrt{a}}\exp(ikx\sin\theta)\,dx, \quad n = 0 \\ C_n &= \int_{-a/2}^{a/2} \sqrt{\frac{2}{a}}\cos\left(\left[\frac{n\pi}{a}\right]\left[x + \frac{a}{2}\right]\right) \\ &\quad \cdot \sqrt{\frac{2}{a}}\exp(ikx\sin\theta)\,dx, \quad n > 0. \end{aligned} \tag{16}$$

It is important to remember that C_n approximates the amplitude of the down-going mode within the groove at $z = 0$ for the given incident wave with z dependence $\exp(ik_{zn}z)$. It is invariant in x as Eq. (18) it is an amplitude of the nth modal component. In reality, the field and hence impedance will vary in x across the aperture because of the combination of different x-axis spatial frequencies of each mode. The field across the aperture is approximated by considering only the modal amplitude C_n, which will result in an x invariant lumped average modal velocity.

The average down-going component of velocity at the origin, v_{zn}^- is simply

$$\begin{aligned} v_{zn}^- &= C_n \exp(ik_{zn}^- z) \\ &= C_n, \quad z = 0. \end{aligned} \tag{17}$$

With knowledge of the impedance of the nth-mode, the corresponding pressure quantity at the origin is defined thus, where k is the wave number of the incident wave

$$p_n^- = v_{zn}^- Z_C \frac{k}{k_{zn}^-}, \quad x = z = 0. \tag{18}$$

The down-going wave is denoted by the k_{zn}^- term, maintaining the correct inverse sign relationship between p_n^- and v_n^- for down-going propagation. The up-going components are the reflections from the bottom surface of the groove and hence will have traversed the full depth of the groove twice. The reflected component of velocity is expressed as follows, where the -1 factor accounts for the phase inversion upon reflection from the bottom and the two exp() phase factors account for the downward and upward traverse, respectively,

$$\begin{aligned} v_{zn}^+ &= C_n \exp\left(ik_{zn}^-(-h)\right) \exp\left(ik_{zn}^+ h\right)(-1) \\ &= -C_n \exp\left(ik_{zn}^+ 2h\right). \end{aligned} \tag{19}$$

The expansion is completed with the reflected pressure component where the $Z_C(k/k_{zn}{}^+)$ term remains positive as it is up-going,

$$\begin{aligned} p_n^+ &= v_{zn}^+ Z_C \frac{k}{k_{zn}^+} \\ &= v_{zn}^+ Z_C \frac{k}{k_{zn}^+}. \end{aligned} \tag{20}$$

Substituting the expansions into Eq. (15), summing over all n-modes and normalising to Z_c and accounting for apparent porosity with the factor a/d provides the approximate expression for the effective impedance within the groove, thus

$$Z_{eff} = \frac{a}{d}\left(\frac{\sum_{n=0}^{n=\infty} C_n\left(\frac{k}{k_{zn}^-} - \exp\left(ik_{zn}^+ 2h\right)\frac{k}{k_{zn}^+}\right)}{\sum_{n=0}^{n=\infty} C_n\left(1 - \exp\left(ik_{zn}^+ 2h\right)\right)\cdot d\boldsymbol{n}}\right). \tag{21}$$

Our velocity components are already posed in terms of vertical velocity, so the $d\mathbf{n}$ term in Eq. (21) equates to -1. For practical application, n must be truncated to N, so, for instance, truncating to $N = 2$ will model the first three cavity modes within the groove from $n = 0$ to $n = 2$. Truncation of N should be chosen such that the upper frequency bound of interest is lower than the cut-off frequency of mode $N + 1$. The upper frequency limit of the simplified model for a given truncation N is, therefore,

$$f_{\max} = \frac{c_0(N+1)}{2a}. \tag{22}$$

This ensures that all propagating cavity modes are included within the frequency range of interest.

A. Simple summation model

This section introduces a series of heuristic steps so the result is a simplified heuristic analytical approximate impedance model for the rectangular grooved surface. Expanding upon the result of Eq. (21) an $N + 1$ term summation based approximation may be formed to include higher order groove modes. This requires each term to be independent, thereby neglecting interaction between modes within the grooves and prohibiting a Real part of the effective impedance due to coupling between modes. The approximation is a weighted impedance summation as opposed to wave superposition as in Eq. (21), and scattering losses will be approximated within the imaginary part of the resulting effective impedance.

Begin with the impedance for mode-n within each groove Z_n, normalise by Z_C, and multiply by the surface normal $d\mathbf{n}$ (-1 in this case) as the impedance of a surface is being expressed to give

$$Z_n = i\frac{k}{k_{zn}^+}\cot(k_{zn}^+ h). \tag{23}$$

The approximate effective impedance is, therefore, the $W_n(\omega)$ weighted sum of all n-modes, the weighting required to account for the frequency dependent excitation of each mode, which depends upon the energy transferred to each mode from the incident wave and the modal impedance. Consistent with the work of Kelders *et al.*,[7,9] the groove depth correction of $h{:}h_0 = h\text{-}a/\pi\ log2$ was employed for the plane wave mode $n = 0$ term alone. It was presented by Hurd[35] for a parallel problem in electromagnetics as a depth correction in rectangular grooved diffraction gratings. Once again, a porosity factor of a/d is included for each term. Given this, and noting that the leading k/k_{zn}^+ term equates to unity for $n = 0$, gives the summation

$$\begin{aligned} Z_{effs} = {} & W_0(\omega)\frac{d}{a} i\cot(k_{z0}^+ h_0) \\ & + \sum_{n>0} W_n(\omega)\frac{d}{a}\cdot\frac{k}{k_{zn}^+} i\cot(k_{zn}^+ h). \end{aligned} \tag{24}$$

Allard *et al.*[9] presented a Low-frequency impedance approximation (LFA), which has the same form as the zeroth term of our simple summation model and will be discussed in Sec. IV B. The $h{:}h_0$ correction factor is compensating the impedance of the groove for the effect of higher order modes in the low frequency region where they are evanescent and is quite different from the classical "organ pipe" end correction for quarter wavelength resonances. Furthermore, the $h{:}h_0$ correction is not applicable to the modal model of Sec. II A because the salient higher order modal effects are implicit within the complexities of the modal model itself, and this correction is intended to compensate simplified low-frequency models for higher order modal effects.

B. Weighting function

The C_n function of Eq. (16) may be used as a basis of the frequency dependent weighting function $W_n(\omega)$. As the modes are fully decoupled, the relative phase of C_n is

https://doi.org/10.1121/10.0000490

redundant, and so only the magnitude is required to give a scalar weighing envelope for each mode. As will be justified later, the effective impedance tends to be dominated by the behaviour of the highest order propagating mode (real k_{zn}), and so the periodic resonances from the *cot* term relating to lower order modes tend to create false peaks in the response. Contributions from lower order modes are thus removed by forcing $W_n(\omega)$ to zero. In its crudest form, this may be achieved by nulling any contribution from mode n when mode $n+1$ is propagating. The $W_n(\omega)$ function is expressed as

$$W_n(\omega) = |C_n| \frac{i\,\mathrm{Im}\{k^+_{zn+1}\}}{k^+_{zn+1}}, \tag{25}$$

where

$$\frac{i\,\mathrm{Im}\{k_{zn+1}\}}{k_{zn+1}} \equiv \begin{cases} 0 & |\mathrm{Re}\{k_{zn+1}\}| > 0 \\ 1 & else, \end{cases} \tag{26}$$

which has the effect of removing the contribution of mode n, once the next highest mode $n+1$ becomes propagating. When h is small compared with a, the behaviour of the total field is dominated by near-field effects which are mitigated by using the aforementioned $h{:}h_0$ correction. For a given source-receiver geometry, the relationship between h and a also determines the relative influences of path length difference and scattering because the path length difference minima will be most influenced by h whereas scattering has a dependence on a (via its relationship to d). The smaller the depth of the groove h, the higher in frequency the first path length difference excess-attenutaion (EA) minima will be. Conversely, increasing a (and d proportionally) will lower the frequency at which scattering effects occur. Thus, increasing a and reducing h will close the frequency gap between the first path length difference EA minimum and the onset of scattering.

While being significantly less computationally demanding than BEM, as an engineering model, the full inner product formulation of C_n Eq. (16) is cumbersome to implement due to the need to compute inner products. The C_n set will, therefore, be approximated with an analytic approximation which assumes grazing incidence so that the $\sin(\theta)$ term in the exp() vanishes. In addition, unit porosity $a = d$ is assumed for the C_n set as porosity terms have already been included in the summation. This gives the grazing incidence analytic approximation for $|C_0|$ of

$$|C_0| \approx \frac{2\sin\left(\frac{a\,k}{2}\right)}{a\,k}, \quad n = 0,\ \theta = \pi/2. \tag{27}$$

As the concern is only with the magnitude of C_n, then for $n > 0$, $|C_n|$ may be approximated by considering the relationship purely in terms of relative x-axis projected wavelength of the incident wave λ_i and that of mode n within the groove aperture λ_n. The $|C_n|$ function is proportional to the sine of the ratio of the two wavelengths, exhibiting a peak when the two wavelengths are nearly equal. The inner product is an area integral so the peak value does not occur when the wavelengths are exactly the same except for the limiting case, where the inner product is conducted over an infinite number of cycles. A wavelength factor Λ_n must, therefore, be included to account for this fact. Our approximation to $|C_n|$ for $n > 0$ is as follows:

$$|C_n| \approx \sin\left(\left[\frac{\lambda_n}{\Lambda_n\,\lambda_i}\right]\frac{\pi}{2}\right), \quad n > 0, \tag{28}$$

where the x projected wavelengths are given by

$$\begin{aligned} \lambda_n &= 2a/n, \\ \lambda_i &= \left(\frac{k\sin\theta}{2\pi}\right)^{-1}. \end{aligned} \tag{29}$$

Combining these gives the simple approximate expression for $|C_n|$ for $n > 0$ of

$$\begin{aligned} |C_n| &\approx \sin\left(\left[\frac{2a/n}{\Lambda_n\left(\frac{k\sin\theta}{2\pi}\right)^{-1}}\right]\frac{\pi}{2}\right) \\ &\approx \sin\left(\frac{a\,k\sin\theta}{2\Lambda_n\,n}\right), \quad n > 0. \end{aligned} \tag{30}$$

The constant Λ_n has periodic solutions, but the particular solution required is the peak value in the region of equality of λ_i and λ_n and is given by the solution of

$$\frac{d|C_n|}{d\Lambda_n} = 0, \quad n > 0, \tag{31}$$

where the full equation for $|C_n|$ as in Eq. (16) must be solved. The solution is independent of a, so it is possible to set $a = 2$ for convenience as this cancels the leading $(2/a)^{0.5}$ terms, giving

$$\begin{aligned} &\frac{d}{d\Lambda_n}\left|\int_{-1}^{1}\cos\left(\left[\frac{n\pi}{2}\right][x+1]\right).\exp\left(i\,x\Lambda_n k\sin\theta\right)dx\right| \\ &\quad = 0, \quad a = 2. \end{aligned} \tag{32}$$

Setting λ_i and λ_n to be equal in order to allow the solution of Λ_n requires

$$\begin{aligned} \lambda_n &= \lambda_i, \\ \frac{2a}{n} &= \left(\frac{k\sin\theta}{2\pi}\right)^{-1}, \\ \frac{\pi n}{a} &= k\sin\theta. \end{aligned} \tag{33}$$

Substituting Eq. (33) into Eq. (32) gives the equation of Λ_n, which is solved within the given interval to remain in the region of interest and exclude periodic higher order correlation peaks

$$\frac{d}{d\Lambda_n}\left|\int_{-1}^{1}\cos\left(\left[\frac{n\pi}{2}\right][x+1]\right).\exp\left(ix\Lambda_n\frac{\pi n}{2}\right)dx\right|=0,$$
$$a=2,\quad 1.5\geq\Lambda_n\geq 1. \tag{34}$$

With the aid of wolfram alpha,[36] the approximate solutions are shown below in Table I for $n=1$ through $n=6$. They clearly show the tendency to unity with increasing n, as to be expected, as the correlation window of $\pm a$ encompasses ever more cycles.

C. Slit-pore model as zeroth term

When the wavelength is large compared with the groove width and the boundary layer thickness is comparable with the semi-width of a, then the thermal viscous effects are at their most significant and accuracy may be improved if the zeroth order term is replaced by the impedance of a hard-backed slit-pore layer (see Sec. IV A). Substituting the slit-pore model as the zeroth term gives

$$Z_{effs}=Z_{SP}(h_0)\,W_0(\omega)+\sum_{n>0}W_n(\omega)\frac{d}{a}.\frac{k}{k_{zn}^{+}}i\cot(k_{zn}^{+}h), \tag{35}$$

where, once again, the $h{:}h_0$ correction is used for the $n=0$ mode which is now the slit-pore term. This represents an approximate effective impedance model for a rectangular grooved grating, valid over a broad frequency range for a given groove geometry and appropriate truncation of N. When the incident wavelength is long when compared to groove dimensions, visco-thermal effects will be significant but only the plane wave mode will be dominant and scattering effects negligible. Conversely, when the wavelength is short compared to the groove dimensions diffractive, scattering and modal behaviour will be dominant. The formulation of a simple analytic impedance model for the rectangularly grooved surface structure which includes diffractive effects is believed to be novel.

D. Truncating *N*

The truncation of N should be chosen such that the maximum frequency of interest is lower than the cut-off frequency of mode $N+1$. This ensures that all modes capable of propagation within the grooves are included in the simple summation across the bandwidth of interest. With reference to Eq. (22), the following inequality is derived and should be satisfied to estimate a sensible truncation of N. Mode n may propagate within the groove whenever the incident wavelength λ_i is shorter than $2a$ because aperture modes are resonant at each half cycle. For a chosen maximum frequency f_{max}, an inequality is formed around N and f_{max} as follows:

$$\lambda_i<\frac{2a}{N+1},$$
$$f_{\max}<\frac{c_0(N+1)}{2a},$$
$$N>\frac{2af_{\max}}{c_0}-1,\quad N=0,1,2,\ldots. \tag{36}$$

N should be rounded up to the next highest integer to ensure there are sufficient summation terms for a given f_{max}.

TABLE I. Approximate solutions of Λ_n.

n	$\sim\Lambda_n$
1	1.367
2	1.125
3	1.06
4	1.035
5	1.025
6	1.02

IV. SIMPLE MODELS FOR EFFECTIVE IMPEDANCE

A. The slit-pore model

The slit-pore model assumes the ground surface to be comprised of narrow parallel walled slits of a given depth when compared to an incident wavelength, backed by an acoustically hard layer. The normalised impedance is given below in terms of complex compressibility $C(\omega)$ and density $\rho(\omega)$ functions[29–31]

$$Z_{SP}(h)=\left(\frac{1}{\rho_0c_0}\sqrt{\frac{q}{\Omega^2}.\frac{\rho(\omega)}{C(\omega)}}\right)\coth\left(-i\omega h\sqrt{q\rho(\omega)C(\omega)}\right) \tag{37}$$

where for slit–pores,

$$\rho(\omega)=\frac{\rho_o}{1-\left((a/2)\sqrt{\omega/c_0}\sqrt{-i}\right)^{-1}\tanh\left((a/2)\sqrt{\omega/c_0}\sqrt{-i}\right)},$$
$$C(\omega)=(\gamma P_o)^{-1}\left(1+\frac{(\gamma-1)}{\sqrt{-iN_{pr}}(a/2)\sqrt{\omega/c_0}}\times\tanh\left(\sqrt{-iN_{pr}}(a/2)\sqrt{\omega/c_0}\right)\right),$$
$$N_{pr}=\text{Prandtl Number}\approx 0.708,$$
$$\gamma=\text{Adiabatic gas constant}\approx 1.41.$$

The parameters are defined thus and apply to the 2D grooved structure of Fig. 1:

Porosity, $\Omega=a/d$.
Tortuosity, $q=1$.

Tortuosity is unity in accordance with the straight parallel rectangular grooves and the flow resistivity is calculated for slit shaped pores according to the equation

$$R_S=\frac{2\mu q^2 s_0}{\Omega r_h^2},$$
$$\mu=\text{dynamic viscosity coefficient of air}=1.811\times10^{-5},$$
$$s_0=\text{shape factor for slit}-\text{pores}=1.5,$$
$$r_h=\text{hydraulic radius for slit}-\text{pore}=a/2. \tag{38}$$

https://doi.org/10.1121/10.0000490

B. LFA impedance model for a groove

The low-frequency model presented by Allard *et al.*[9] for an isolated rectangular groove at normal incidence can be derived from the modal model with the limiting truncation of $N=M=0$ and by definition includes the $h{:}h_0$ groove depth correction. The effective normalised impedance according to the LFA is

$$Z_{AKL}=\frac{i}{\Omega}\cot\left(k\left[h-\frac{a}{\pi}\log 2\right]\right). \tag{39}$$

It is clear that the slit-pore and LFA models may cease to hold if any scattered mode is free-space propagating because they assume purely specular reflection. Between normal and grazing incidence, every scattered field exhibiting free-space propagation will include the $m=-1$ mode, which infers the general condition of validity for the slit-pore and LFA models of

$$|\alpha_{-1}|\leq|k|,\quad \pi/2\geq\theta>0. \tag{40}$$

For a given geometry, this represents a high frequency scattering limit f_{LS} above which scattering will occur and the homogeneous ground assumption, upon which the slit-pore and LFA models rely, will cease to hold. The groove depth h and aperture width a (strictly speaking only by virtue of affecting d), will influence the magnitude of the scattered components but not their propagation characteristics. Therefore, the slit-pore and LFA models may hold outside of the limits imposed by Eq. (40) if the magnitudes of scattered components are negligible, such as when $h\to 0$, $a\to 0$, or $a/d\to 0$. Extensive testing has shown that the condition of Eq. (40) represents a high frequency limit of the slit-pore model, above which it may be in significant error due to the onset of scattering. Furthermore, and as can be seen later, the slit-pore and particularly the LFA model may also tend to increase error to a greater or lesser degree depending upon the geometry as f_{LS} is approached, where the effects of higher order modes become significant.

The simple summation model of Eq. (35) will overcome the scattering limitation of Eq. (40) as it approximates scattering effects by considering higher order modes within the grooves. It includes the slit-pore model as its zeroth term and so visco-thermal effects will be included for the plane-wave mode within the groove, which is the realm where such effects will be dominant. Thus, it may be argued that if one were to introduce visco-thermal effects for the higher order modes, it would be of diminishing value as visco-thermal and scattering effects dominate under opposing conditions.

C. Comparison with BEM predictions

In this section, the results from the modal model and effective impedance models are compared with those from BEM at two extremes of the a/d ratio, 1/6 and 5/6. Parameters for the BEM simulations are a mesh resolution of 0.008 m with acoustically hard surfaces and the grating extending horizontally beyond the source and receiver. Source and receiver heights are specified as the height above the highest extent of the grating structure. Figure 4 shows a summary of the close agreement of the BEM and modal models for two cases. The plots show predicted EA spectra (defined as the total sound field with respect to the free-field) for the five models.

Agreement of the modal model with BEM in Fig. 4(a) is excellent throughout the spectrum. The effective impedance model of the cot() series summation [using Eq. (35) with approximated inner products of Eqs. (27) and (30)] shows good agreement with BEM. Whereas the slit-pore model loses accuracy beyond f_{LS} and fails to predict the second EA minima entirely. The LFA model is unreliable throughout, but this is not surprising as it is not intended to be applied near grazing incidence nor in the realm of scattering. The causal model of Eq. (21) shows generally poor performance in Fig. 4(a) but fares better in Fig. 4(b). For Fig. 4(b), only the full modal model is in agreement with the BEM as to the frequency of the first EA minimum and all except the modal model begin to loose accuracy with BEM from around 1 kHz prior to f_{LS} for this particular geometry and hence fail to correctly predict the frequency of the first EA minimum. However due to the low a/d ratio of Fig. 4(b), all models regain agreement beyond f_{LS}. The standard errors (SEs) for each model prediction with

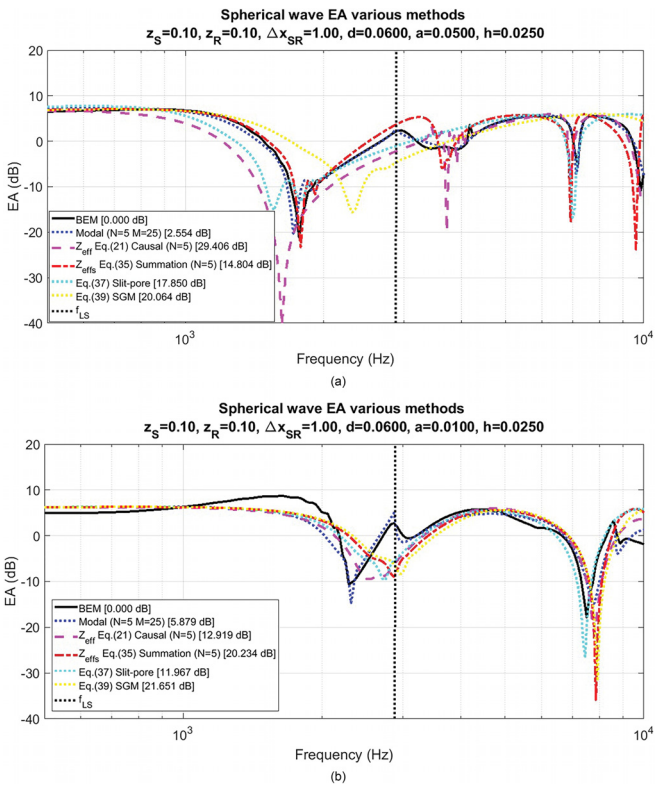

FIG. 4. (Color online) (a) Simulated EA spectra for $d=0.06$, $a=0.05$, $h=0.025$, and 0.1 m source-receiver heights separated by 1 m. (b) Simulated EA spectra for $d=0.06$, $a=0.01$, $h=0.025$, and 0.1 m source-receiver heights separated by 1 m.

reference to the BEM model and using the following formula can be calculated as a measure of goodness of fit, although these figures can be distorted:

$$SE = \sqrt{\frac{1}{n}\sum_{f_n} |EA_{measurement}(f_n) - EA_{predicted}(f_n)|^2}. \tag{41}$$

D. Comparison with measurement

Measurements were made in an anechoic chamber using one metre wide aluminium strips placed upon a hard surface to create a groove grating structure protruding above ground with different values of a/d and with the grating extending horizontally between the source and receiver. A personal computer running a single MATLAB script was used as a host to generate the signal waveforms and to collect and post process the data via a National Instruments data acquisition module (DAQ) connected by USB. The sound source was a Tannoy driver acoustically coupled to a 22 mm diameter copper tube with length L_T of 2.2 m to approximate a point source and driven by the DAQ via an audio amplifier with a short duration impulse as the excitation. The receiver was a Brüel & Kjær 0.5 in. free field microphone cartridge type 4966 with an amplifier type 2669 and model 5935 battery power supply. The analogue output from the preamplifier was and band-pass filtered and sampled by the DAQ and the data stream acquired by the host computer via the USB link. A block diagram of the hardware set-up used to make the measurements is given in Fig. 5.

The data from many impulse signal bursts were post processed in the MATLAB script being subject to windowing to remove stray reflections and averaging to improve the signal to noise ratio. Finally, a fast Fourier transform (FFT) was applied to obtain the frequency response of the system. The EA spectrum was obtained by first measuring the system with the layer under test (LUT) removed and the source and microphone lowered very close to, but not touching, the hard ground surface while maintaining the same horizontal separation to obtain a reference measurement of the environment. Full measurements were then taken with the LUT in place and the source and receiver in their prescribed locations as in Fig. 5. The resulting EA spectrum for the grating surface under test was therefore obtained from

$$EA(f)_{dB} = 20\log_{10}\left(\frac{\text{Full measurement}(f)}{\text{Reference measurement}(f)}\right) \text{ dB}. \tag{42}$$

Figures 6(a) and 6(b) compare EA spectra predicted by the modal, the simple summation approximation with the slit-pore zeroth-term of Eq. (35) with the approximated inner products of Eqs. (27) and (30), and the slit-pore and LFA models with laboratory data. The measurement results were not sensitive to the horizontal placement of the grooves in respect of whether the source or receiver are placed over a gap between the strips or the top of a strip.

The resulting EA spectra for the slit-pore and LFA impedance models tend to be unreliable beyond f_{LS}, but show increasing accuracy below this point as neither account for scattering effects. As would be expected, the slit-pore layer and LFA models exhibit their best

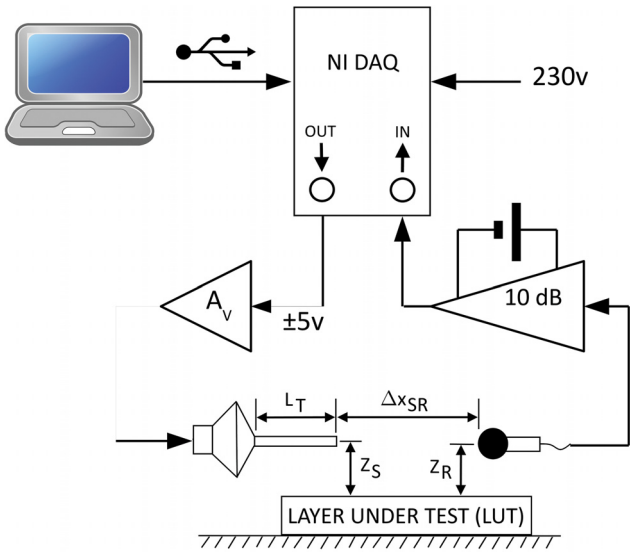

FIG. 5. (Color online) Measurement setup.

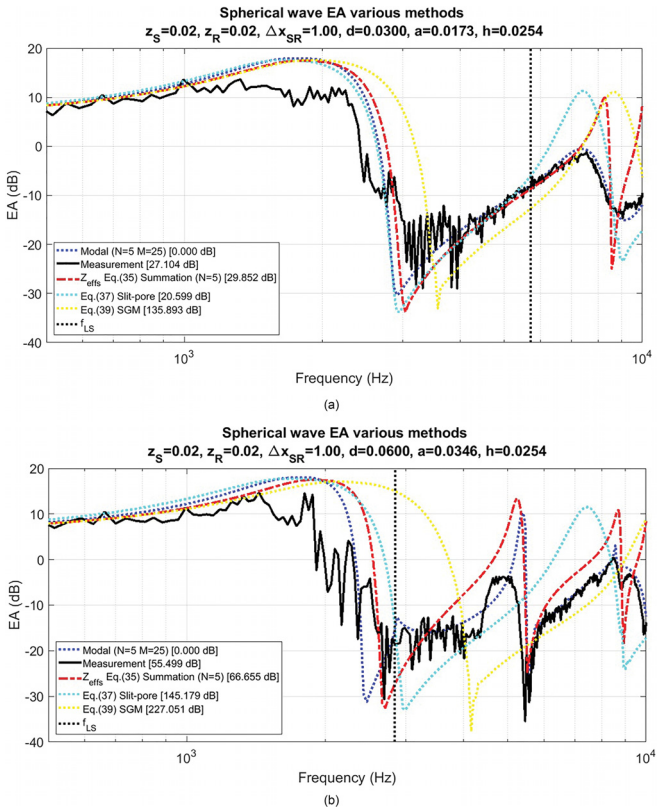

FIG. 6. (Color online) (a) Measured and predicted EA spectra for $d = 0.030$, $a = 0.017$, $h = 0.025$. (b) Measured and predicted EA spectra for $d = 0.060$, $a = 0.035$, and $h = 0.025$.

https://doi.org/10.1121/10.0000490

agreement with data in Fig. 6(a), where the groove is at its narrowest and scattering effects do not occur in the lower region of the spectrum. It would be sensible to think that in the region of the first EA minima and far below f_{LS} where scattering effects will be negligible, the slit-pore will be the most accurate model [Fig. 6(a)] due to its inclusion of thermo-viscous losses. The underestimating of the surface wave component in the measurements is likely due to experimental error due to the non-ideal reproduction of the structure.

The modal model shows generally good agreement throughout the range of data. It is especially suited to cases dominated by scattering behaviour [Fig. 6(b)] and remains accurate even when a is less than or comparable to h and the effective porosity a/d is significantly less than unity.

The series model shows a good prediction of the frequencies of EA maxima and minima across the spectrum. The magnitude of the response is routinely overestimated beyond f_{LS} because the groove modes in the series model have been decoupled and so do not destructively interfere to produce negative real parts which would suitably account for scattering losses.

E. Testing the approximations

Given grazing incidence, the highest order propagating n-mode has the potential to receive the most excitation energy from the incident wave because of the similarity in x-axis spatial frequency. Although lower order modes may still be excited, their potential excitation energy will be ever decreasing with frequency due to their inner product being only proportional to the area of one incident half cycle. It may, therefore, be shown in Fig. 7 that the highest order propagating mode tends to dominate the local response while at the same time asserting that the simplifications of Eqs. (27)–(30) to the full inner product are reasonable.

The errors of the approximate inner products as shown in Fig. 7(a) are small in the region around the associated cut-off frequency (denoted by the corresponding vertical cursor) and upto the cut-off frequency of the next higher mode. Throughout the remaining spectrum, however, the approximations exhibit large errors. Despite this, the predicted EA curves from both the full and approximate inner products in Fig. 7(b) are in close agreement suggesting that the local response is dominated by the highest order propagating mode and that our treatments of approximating the inner product are reasonable.

V. CONCLUSIONS

A modal model has been used to derive an approximate effective impedance for a regularly grooved acoustically hard surface. When applied to point-to-point propagation, it shows good agreement with BEM calculations and measurements but requires significantly less computation. The modal model is, however, limited to rectangular grooved gratings whereas BEM will apply to any shape. Implementation of the modal model, although simpler than BEM, is not a trivial

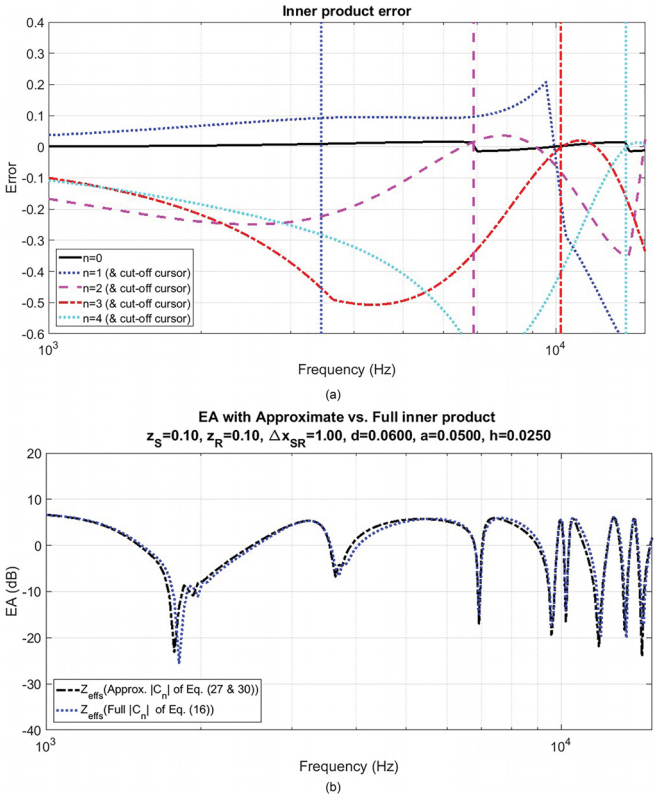

FIG. 7. (Color online) (a) Approximated inner product error curves with respect to the full inner product for the first 5 n-modes [Eqs. (16)–(27) or (30)]. (b) Comparison of EA curve prediction of summation model Eq. (35) using the full inner products of Eq. (16) and simplified versions of Eqs. (27) and (30).

task and so may preclude practical application in many acoustic engineering problems. An approximate model has been derived for engineering applications. Such an application of the modal model is believed to be novel.

Inspired by the modal model methods, a new analytic series approximation to the effective impedance of a rectangularly grooved grating is presented. Using the slit-pore model as the zeroth (low-frequency) term, the model is more accurate than the slit-pore model alone for a wider range of aperture to depth ratios including those for which there is significant scattering. Moreover, it offers an engineering model for predicting point-to-point propagation over a grooved surface for which there is no simple analytical model.

Using the modal model and its approximations, a rigorous method for determining the range of applicability of the slit-pore model has been presented, whose validity is limited by the onset of scattering. Prior to this, the limits of the slit-pore model had been explored in an empirical way using a restricted set of laboratory measurements.[1]

Ongoing work includes extending the modal model to predict the acoustic field above three-dimensional (3D) latticed ground structures for any azimuthal angle with a view to extending the simple summation model to predict the effective impedance of a lattice. Modelling a Real part to the higher order mode impedance terms of the simple

summation model is also of interest. Stinson[37] extended the work of Kirchoff *et al.*[38] to predict oscillatory flow in a rectangular tube for all supported modes so it would be of interest to reconcile this work with ours. Extending the modal model to predict the response of rectangular grooved metasurfaces where each grating period consists of several grooves of different depths is also of interest for future effort.

[1]I. Bashir, "Acoustical exploitation of rough, mixed impedance and porous surfaces outdoors," Ph.D. thesis, Open University, Milton Keynes, UK, 2013.
[2]S. Taherzadeh, I. Bashir, T. Hill, K. Attenborough, and M. Hornikx, "Reduction of surface transport noise by ground roughness," Appl. Acoust. **83**, 1–15 (2014).
[3]I. Bashir, S. Taherzadeh, and K. Attenborough, "Surface waves over periodically spaced strips," J. Acoust. Soc. Am. **134**, 4691–4697 (2013).
[4]I. Bashir, S. Taherzadeh, and K. Attenborough, "Diffraction-assisted rough ground effect: Models and data," J. Acoust. Soc. Am. **133**, 1281–1292 (2013).
[5]M. S. Tong, L. Y. Ting, W. C. Chew, and M. J. White, "A study for sound wave scattering by corrugated ground with complex trench structures," Waves Random Complex Media **19**, 392–408 (2009).
[6]W.-T. Ang, *A Beginner's Course in Boundary Element Methods* (Universal Publishers, Boca Raton, FL, 2007).
[7]L. Kelders, J. F. Allard, and W. Lauriks, "Ultrasonic surface waves above rectangular-groove gratings," J. Acoust. Soc. Am. **103**(5), 2730–2733 (1998).
[8]A. Hessel, J. Schmoys, and D. Y. Tseng, "Bragg-angle blazing of diffraction gratings," J. Opt. Soc. Am. **65**(4), 380–384 (1975).
[9]R. Porter and D. V. Evans, "Embedded Rayleigh-Bloch surface waves along periodic rectangular arrays," Wave Motion **43**, 29–50 (2005).
[10]J. Christensen, A. I. Fernandez-Dominguez, F. De Leon-Perez, L. Martin-Moreno, and F. J. Garcia-Vidal, "Collimation of sound assisted by acoustic surface waves," Nat. Phys. Lett. **3**, 851–852 (2007).
[11]Y. Zhou, M. H. Lu, L. Feng, X. Ni, Y. F. Chen, Y. Y. Zhu, S. N. Zhu, and N. B. Ming, "Acoustic surface evanescent wave and its dominant contribution to extraordinary acoustic transmission and collimation of sound," Phys. Rev. Lett. **104**, 164301 (2010).
[12]Z. He, H. Jia, C. Qiu, Y. Ye, R. Hao, M. Ke, and Z. Liu, "Nonleaky surface acoustic waves on a textured rigid surface," Phys. Rev. B **83**, 132101 (2011).
[13]L. Quan, X. Zhong, X. Liu, X. Gong, and P. A. Johnson, "Effective impedance boundary optimization and its contribution to dipole radiation and radiation pattern control," Nat. Commun. **5**, 3188 (2014).
[14]J. Lu, C. Qiu, M. Ke, and Z. Liu, "Directional excitation of the designer surface acoustic waves," Appl. Phys. Lett. **106**, 201901 (2015).
[15]X. D. Fan, Y. F. Zhu, B. Liang, J. Yang, L. Yin, J. Yang, and J. C. Cheng, "Three-dimensional ultra-broadband focusing flat mirror for airborne sound," Appl. Phys. Lett. **109**, 153501 (2016).
[16]M. R. Schroeder, "Binaural dissimilarity and optimum ceilings for concert halls: More lateral sound diffusion," J. Acoust. Soc. Am. **65**, 958–963 (1979).
[17]T. Wu, T. J. Cox, and Y. W. Lam, "From a profiled diffuser to an optimized absorber," J. Acoust. Soc. Am. **108**, 643–650 (2000).
[18]D. Torrent and J. Sanchez-Dehesa, "Acoustic analogue of graphene: Observation of dirac cones in acoustic surface waves," Phys. Rev. Lett. **108**, 174301 (2012).
[19]J. Zhu, Y. Chen, X. Zhu, F. J. Garcia-Vidal, X. Yin, W. Zhang, and X. Zhang, "Acoustic rainbow trapping," Sci. Rep. **3**, 1728 (2013).
[20]Y. Zhu, X. Y. Zou, B. Liang, and J. C. Cheng, "Acoustic one-way open tunnel by using metasurface," Appl. Phys. Lett. **107**, 113501 (2015).
[21]Y. F. Zhu, X. Y. Zou, R. Q. Li, X. Jiang, J. Tu, B. Liang, and J. C. Cheng, "Dispersionless manipulation of reflected acoustic wavefront by subwavelength corrugated surface," Sci. Rep. **5**, 10966 (2015).
[22]L. Schwan, A. Geslain, V. Romero-Garcia, and J. P. Groby, "Complex dispersion relation of surface acoustic waves at a lossy metasurface," Appl. Phys. Lett. **110**, 051902 (2017).
[23]L. Schwan, O. Umnova, and C. Boutin, "Sound absorption and reflection from a resonant metasurface: Homogenisation model with experimental validation," Wave Motion **72**, 154–172. (2017).
[24]C. M. Linton and I. Thompson, "Resonant effects in scattering by periodic arrays," Wave Motion **44**, 165–175 (2007).
[25]S. Yves, R. Fleury, F. Lemoult, M. Fink, and G. Lerosey, "Topological acoustic polaritons: Robust sound manipulation at the subwavelength scale," New J. Phys. **19**, 075003 (2017).
[26]D. L. Berry, S. Taherzadeh, and K. Attenborough, "Acoustic surface wave generation over rigid cylinder arrays on a rigid plane," J. Acoust. Soc. Am. **146**, 2137–2144 (2019).
[27]R. Zhao, T. Liu, C. Y. Wen, J. Zhu, and L. Cheng, "Impedance-near-zero acoustic metasurface for hypersonic boundary-layer flow stabilization," Phys. Rev. Appl. **11**, 044015 (2019).
[28]J. F. Allard, L. Kelders, and W. Lauriks, "Ultrasonic surface waves above a doubly periodic grating," J. Acoust. Soc. Am. **105**(4), 2528–2531 (1999).
[29]K. Attenborough, I. Bashir, and S. Taherzadeh, "Outdoor ground impedance models," J. Acoust. Soc. Am. **129**(5), 2806–2819 (2011).
[30]K. Attenborough, K. M. Li, and K. Horoshenkov, *Predicting Outdoor Sound* (Taylor and Francis, London, 2007).
[31]Y. Champoux and M. R. Stinson, "On acoustical models for sound propagation in rigid frame porous materials and the influence of shape factors," J. Acoust. Soc. Am. **92**(2), 1120 (1992).
[32]I. Tolstoy, "Smoothed boundary conditions, coherent low-frequency scatter, and boundary modes," J. Acoust. Soc. Am. **75**, 1 (1984).
[33]C. F. Chien and W. W. Soroka, "Sound propagation along an impedance plane," J. Sound Vib. **43**(1), 9–20 (1975).
[34]S. W. Rienstra and A. Hirschberg, *An Introduction to Acoustics, Extended and Revised Edition of IWDE 92-06* (Eindhoven University of Technology, Eindhoven, the Netherlands, 2016).
[35]R. A Hurd, "The propagation of an electromagnetic wave along an infinite corrugated surface," Can. J. Phys. **32**, 727–734 (1954).
[36]See information at www.wolframalpha.com.
[37]M. R. Stinson, "The propagation of plane sound waves in narrow and wide circular tubes, and generalization to uniform tubes of arbitrary cross-sectional shape," J. Acoust. Soc. Am. **89**, 550–558 (1991).
[38]G. Kirchoff, "Über den Einflufs der Warmeleitung in einem Gase auf die Schallbewegung," Ann. Phys. Chem. **134**, 177–193 (1868).